Advances in Nano Research, *Vol. 8 No. 1 (2020) 69-82*
DOI: https://doi.org/10.12989/anr.2020.8.1.069

Analysis of porous micro sandwich plate: Free and forced vibration under magneto-electro-elastic loadings

Mehdi Mohammadimehr* and Mohammad Meskini

Department of Solid Mechanics, Faculty of Mechanical Engineering, University of Kashan, P.O. Box 87317-53153, Iran

(*Received April 14, 2019, Revised August 11, 2019, Accepted October 26, 2019*)

Abstract. In this study, the free and forced vibration analysis of micro sandwich plate with porous core layer and magneto-electric face sheets based on modified couple stress theory and first order shear deformation theory under simply supported boundary conditions is illustrated. It is noted that the core layer is composed from balsa wood and also piezo magneto-electric facesheets are made of $BiTiO_3$-$CoFe_2O_4$. Using Hamilton's principle, the equations of motion for micro sandwich plate are obtained. Also, the Navier's method for simply support boundary condition is used to solve these equations. The effects of applied voltage, magnetic field, length to width ratio, thickness of porous to micro plate thickness ratio, type of porous, coefficient of porous on the frequency ratio are investigated. The numerical results indicate that with increasing of the porous coefficient, the non-dimensional frequency increases. Also, with an increase in the electric potential, the non–dimensional frequency decreases, while and with increasing of the magnetic potential is vice versa.

Keywords: free and forced vibration; electric and magnetic fields; micro sandwich plate; Balsa wood; porous material

1. Introduction

Due to the increasing development in science and technology, the use of intelligent materials such as piezo and porous has been developed by many researchers. In recent years, the studies have been carried out on the vibrations and buckling of plate at micro/nano scales that composed of piezo and porous materials, in which, some investigations have been presented in these researches. Mohammadimehr *et al*. (2014) studied the buckling and free vibration analysis of the double-bonded nanocomposite piezoelectric plate based on modified couple stress theory under electro-thermo-mechanical loadings surrounded by an elastic foundation that reinforced by a boron nitride nanotube. Also, based on Kirchhoff plate theory and the Eshelby-Mori-Tanaka method and employing Hamilton's principle, the equations of motion are obtained. They concluded that with an increase in the aspect ratio and the dimensionless material length scale parameter, the dimensionless natural frequency increases. Based on the modified couple-stress theory and sinusoidal plate theories, bending and free vibration analysis of a functionally graded piezoelectric microplate under simply supported boundary conditions is studied by Li and Pan (2015). Their results showed that the magnitudes of the transverse central deflection, electric potential, stresses and electric displacement in the horizontal directions of microplate predicted by the modified couple-stress model are smaller than predicted by the classical plate model.

Razavi and Shooshtari (2015) investigated nonlinear free vibration of symmetric laminated rectangular plates based on first order shear deformation theory with considering the von Karman's nonlinear strains and simply supported boundary condition. Also, for electric and magnetic model, the Maxwell's equations are used. Based on Euler–Bernoulli and modified couple stress theory, the effect of finite strain and Von Karman assumptions on the nonlinear free vibration and bending of the symmetrically micro and nano laminated composite beam under thermal environment is studied by Mohandes and Ghasemi (2016). Their results illustrated that the material properties have a remarkable influence on the behavior of the finite strain micro beam. Also, their bending results showed that there is a difference between the finite strain and Von Karman assumptions. Arefi and Zenkour (2016) studied the free vibration, tension analysis and wave propagation of a sandwich micro and nano rod made of piezoelectric materials under electric potential. The numerical results indicated that with increasing of the foundation parameters leads to increase in phase velocity of sandwich micro rod. In another work, they (2017b) investigated the analysis of sandwich beam curve with two piezo magnetic layer face sheet and elastic layer in core based on FSDT. That, they expressed the influence of the applied electric and magnetic potentials on the electro mechanical responses of the beam.

The conductivity of carbon nano fiber or nano tube incorporated cement composite under static and dynamic conditions expressed by Sasmal *et al*. (2017). Also, they investigated the influence of external voltage and Gauge factors of the conductive cement. Mohammadimehr and Alimirzaei (2016) considered nonlinear static and vibration analysis of Euler-Bernoulli composite beam model reinforced by FG-SWCNT with initial geometrical

*Corresponding author, Associate Professor,
E-mail: mmohammadimehr@kashanu.ac.ir

http://www.techno-press.org/?journal=journal=anr&subpage=5
ISSN: 2287-237X (Print), 2287-2388 (Online)

imperfection using FEM. Zhang *et al*. (2018) presented the nonlinear vibrations of composite laminated piezoelectric rectangular plate based on third-order shear deformation plate theory. To analyze the periodic and chaotic motions of the symmetric cross-ply composite laminated piezoelectric rectangular plate, the fourth-order Runge-Kutta algorithm is used. Abazid and Sobhy (2018) studied on the bending of piezoelectric functionally graded microplate under thermos-electro-mechanical loadings. They used MCST and four-variable shear deformation plate theory to derive the equilibrium equations. Also, based on higher-order shear deformation theory and a novel element-free IMLS-Ritz model, the impact analysis of carbon nano tube reinforced piezoelectric composite plate is carried out by Selim *et al*. (2018).

Free vibration analysis of porous plate based on third-order shear deformation plate theory is illustrated by Rezaei and Saidi (2015). They used the Levy-type solution to solve the equation of porous plate with arbitrary boundary conditions. Their results showed that with increasing of the porosity coefficient the natural frequency of fluid free plates decreases. Based on higher order shear deformation theory, the buckling analysis of the FG porous circular plate is presented by Mojahedin *et al*. (2016). The pre-buckling forces and critical buckling loads are determined by Sanders non-linear strain–displacement relation. Their results illustrated that with increasing of the coefficient of porosity, the critical buckling load reduces. Also, the obtained critical buckling load based on the CPT and FSDT are noticeably larger than the values obtained based on the HSDT. Mohammadimehr *et al*. (2017b) considered nonlinear vibration analysis of FG-CNTRC sandwich Timoshenko beam based on modified couple stress theory subjected to longitudinal magnetic field using generalized differential quadrature method (GDQM). Shojaeefard *et al*. (2017) investigated the free vibration and buckling analysis of micro temperature-dependent FG porous circular plates based on MCST, CPT and FSDT under nonlinear thermal load. The FGM layer composed from metal and ceramic materials that the top surface of the plate is metal-rich and the bottom surface is ceramic-rich. Their analysis indicated that the critical temperature change, decreases size dependency and increases the porosity. Mohammadimehr *et al*. (2018) presented free vibration analysis of magneto-electro-elastic cylindrical composite panel reinforced by various distributions of CNTs with considering open and closed circuits boundary conditions based on first-order shear deformation theory (FSDT). The vibration behavior of thick functionally graded porous rectangular plates based on the three-dimensional elastic theory with arbitrary boundary conditions by elastic foundation is expressed by Zhao *et al*. (2018). They showed that the frequency parameter of the FGP plate decreases with increasing of the porosity coefficient. Also, the influence of elastic parameters on the vibration characteristics is investigated.

Based on Donnell shell theory and von-Kármán strain-displacement relation, the nonlinear primary resonance analysis of cylindrical shells made of functionally graded porous materials subjected to a uniformly distributed harmonic load is studied by Gao *et al*. (2018b). Based on first-order shear deformation theory, the buckling behavior of functionally graded graphene reinforced porous nanocomposite cylindrical shells with spinning motion and subjected to a combined action of external axial compressive force and radial pressure is presented by Dong *et al*. (2018). Gao *et al*. (2019) investigated nonlinear dynamic buckling of imperfect beams made of functionally graded metal foams subjected to a constant velocity with various boundary conditions based on von-Karman strain–displacement relation. Mohammadimehr *et al*. (2017c) investigated dynamic stability of modified strain gradient theory sinusoidal viscoelastic piezoelectric polymeric functionally graded single-walled carbon nanotubes reinforced nanocomposite plate considering surface stress and agglomeration effects under hydro-thermo-electro-magneto-mechanical loadings. Wang *et al*. (2019) considered the buckling and post buckling behaviors of graphene platelet reinforced dielectric composite beams based on Timoshenko beam theory and von Karman nonlinear strain-displacement relationship. They obtained the governing equations and then discretized numerically and solved by employing differential quadrature method.

Mohammadimehr *et al*. (2015) depicted surface stress effect on the nonlocal biaxial buckling and bending analysis of polymeric piezoelectric nanoplate reinforced by CNT using eshelby-mori-tanaka approach. In the other work, they (2016) studied size-dependent effect on biaxial and shear nonlinear buckling analysis of nonlocal isotropic and orthotropic micro-plate based on surface stress and modified couple stress theories using differential quadrature method. Ghorbanporur Arani *et al*. (2016) illustrated surface stress and agglomeration effects on nonlocal biaxial buckling polymeric nanocomposite plate reinforced by CNT using various approaches. Cong *et al*. (2018) used the HSDT for the analysis of the nonlinear buckling and post-buckling of the porous FGM plates resting on Winkler–Pasternak model of elastic foundations under thermo-mechanical loadings. Their results illustrated that the increasing of volume fractions, the ceramic constituent decreases, which lead to reduce the plate stiffness and so of the buckling and post buckling resistance capacity. Also, the influence of Pasternak shear layer of the plate is more significantly than the Winkler shears modulus. Arani and Zamani (2018) studied the free vibration of functionally graded porous piezo electric nano plate resting on silica aerogel foundation based on Vlasov’s model foundation based on sinusoidal shear and normal deformation theories. The numerical results indicated that with increasing of the porosity coefficient, the non-dimensional natural frequency decreases. Then, Gao *et al*. (2018a) illustrated the nonlinear free vibration of functionally graded porous nanocomposite plate resting on Winkler-Pasternak elastic foundations with various boundary conditions for different type of porosity distributions. They obtained the equations of motion based on Hamilton’s principle. Also, the differential quadrature method is used to solve these equations. The buckling and free vibration analysis of functionally graded porous nano composite plate based on a multiplayer model is expressed by Yang *et al*. (2018). Their numerical result is shown that with increasing of the porosity coefficient, the fundamental natural frequency decreases. Also, based on MSCT, classical plate theory and first-order shear deformation plate theory, the free vibration, bending and buckling analysis of functionally graded porous micro plate is investigated by Kim *et al*. (2019).

In this research, the effect of electric potential and magnetic fields on the free and forced vibration of piezo magneto-electric micro plate with porous core layer based on modified couple stress and first order shear deformation theory is illustrated. It is noted that the core layer is composed from balsa wood. Based on Hamilton's principle, the equations of motion are obtained. Also, the Navier's method for simply support boundary conditions is used to solve these equations. The effects of applied voltage, magnetic field, length to width ratio, types of porous, coefficient of porous and core layer thickness to micro plate thickness ratio on the natural frequency are investigated.

2. Formulation

Fig. 1 shows the micro sandwich plate with porous core and magneto-electric facesheets that a, b, h_e, h_p, are length, width, thicknesses of core and facesheets, respectively.

In this research, FSDT is used for relations displacements that are defined as (Reddy 2002)

$$\begin{aligned} u(x,y,t) &= u_0(x,y,t) + z\varphi_x(x,y,t) \\ v(x,y,t) &= v_0(x,y,t) + z\varphi_y(x,y,t) \\ w(x,y,t) &= w_0(x,y,t) \end{aligned} \tag{1}$$

where u, v, w, are the displacements along the x, y and z directions, respectively. Also, z is distance from the micro plate middle surface, and u_0, v_0, w_0 are the displacement of the micro plate middle surface. Based on FSDT theory, the normal and shear strains are defined as follows

$$\begin{aligned} \varepsilon_x &= \frac{\partial u}{\partial x} = \frac{\partial u_0}{\partial x} + z\frac{\partial \varphi_x}{\partial x} \\ \varepsilon_y &= \frac{\partial v}{\partial y} = \frac{\partial v_0}{\partial y} + z\frac{\partial \varphi_y}{\partial y} \\ \gamma_{xy} &= \frac{\partial u}{\partial y} + \frac{\partial v}{\partial x} = \frac{\partial u_0}{\partial y} + \frac{\partial v_0}{\partial x} + z\frac{\partial \varphi_x}{\partial x} + z\frac{\partial \varphi_y}{\partial y} \\ \gamma_{xz} &= \frac{\partial u}{\partial z} + \frac{\partial w}{\partial x} = \varphi_x + \frac{\partial w}{\partial x} \\ \gamma_{yz} &= \frac{\partial v}{\partial z} + \frac{\partial w}{\partial x} = \varphi_y + \frac{\partial w}{\partial y} \end{aligned} \tag{2}$$

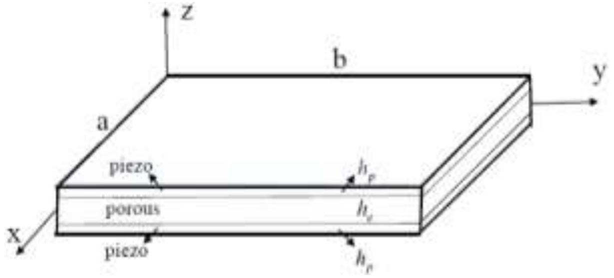

Fig. 1 A shematic view of micro sandwich plate with piezo magneto-electric facesheets and porous core

Also, the constitutive equations for piezo electric and magnetic layers are expressed (Farajpour *et al*. 2016, Arefi and Zenkour 2017a)

$$\begin{Bmatrix} \sigma_x \\ \sigma_y \\ \tau_{xy} \\ \tau_{xz} \\ \tau_{yz} \end{Bmatrix} = \begin{bmatrix} c_{11} & c_{12} & 0 & 0 & 0 \\ c_{12} & c_{22} & 0 & 0 & 0 \\ 0 & 0 & c_{66} & 0 & 0 \\ 0 & 0 & 0 & c_{55} & 0 \\ 0 & 0 & 0 & 0 & c_{44} \end{bmatrix} \begin{Bmatrix} \varepsilon_x \\ \varepsilon_y \\ \gamma_{xy} \\ \gamma_{xz} \\ \gamma_{yz} \end{Bmatrix} - \begin{bmatrix} 0 & 0 & e_{13} \\ 0 & 0 & e_{23} \\ 0 & 0 & 0 \\ e_{51} & 0 & 0 \\ 0 & e_{62} & 0 \end{bmatrix} \begin{bmatrix} E_x \\ E_y \\ E_z \end{bmatrix} - \begin{bmatrix} 0 & 0 & q_{13} \\ 0 & 0 & q_{23} \\ 0 & 0 & 0 \\ q_{51} & 0 & 0 \\ 0 & q_{62} & 0 \end{bmatrix} \begin{bmatrix} H_x \\ H_y \\ H_z \end{bmatrix} \tag{3}$$

where c_{ij}, e_{ij}, q_{ij} are stiffness coefficients of piezo electro magneto material, piezoelectric coefficients and piezo magnetic coefficients, respectively. Also, E_i and H_i denote the electric and the magnetic fields, respectively. Also, electric displacement for electro mechanical system are defined (Farajpour *et al*. 2016, Arefi and Zenkour 2017a)

$$\begin{Bmatrix} D_x \\ D_y \\ D_z \end{Bmatrix} = \begin{bmatrix} 0 & 0 & 0 & e_{15} & 0 \\ 0 & 0 & 0 & 0 & e_{26} \\ e_{31} & e_{32} & 0 & 0 & 0 \end{bmatrix} \begin{Bmatrix} \varepsilon_x \\ \varepsilon_y \\ \gamma_{xy} \\ \gamma_{xz} \\ \gamma_{yz} \end{Bmatrix} + \begin{bmatrix} \in_{11} & 0 & 0 \\ 0 & \in_{22} & 0 \\ 0 & 0 & \in_{33} \end{bmatrix} \begin{bmatrix} E_x \\ E_y \\ E_z \end{bmatrix} + \begin{bmatrix} m_{11} & 0 & 0 \\ 0 & m_{22} & 0 \\ 0 & 0 & m_{33} \end{bmatrix} \begin{bmatrix} H_x \\ H_y \\ H_z \end{bmatrix} \tag{4}$$

where $\in_{ii}$ is the dielectric coefficients and m_{ii} denotes the electromagnetic coefficients. The magnetic displacement for magnetic system are expressed (Arefi and Zenkour 2017a)

$$\begin{Bmatrix} B_x \\ B_y \\ B_z \end{Bmatrix} = \begin{bmatrix} 0 & 0 & 0 & q_{15} & 0 \\ 0 & 0 & 0 & 0 & q_{26} \\ q_{31} & q_{32} & 0 & 0 & 0 \end{bmatrix} \begin{Bmatrix} \varepsilon_x \\ \varepsilon_y \\ \gamma_{xy} \\ \gamma_{xz} \\ \gamma_{yz} \end{Bmatrix} + \begin{bmatrix} m_{11} & 0 & 0 \\ 0 & m_{22} & 0 \\ 0 & 0 & m_{33} \end{bmatrix} \begin{bmatrix} E_x \\ E_y \\ E_z \end{bmatrix} + \begin{bmatrix} \mu_{11} & 0 & 0 \\ 0 & \mu_{22} & 0 \\ 0 & 0 & \mu_{33} \end{bmatrix} \begin{bmatrix} H_x \\ H_y \\ H_z \end{bmatrix} \tag{5}$$

where μ_{ij} is the magnetic coefficients. Also, magnetic and electro fields are defined as the following form (Farajpour *et al*. 2016)

$$\begin{aligned} E_x &= -\frac{\partial \hat{\psi}}{\partial x} = \frac{\partial \psi}{\partial x} cos(\frac{\pi \hat{z}}{h_p}) \\ E_y &= -\frac{\partial \hat{\psi}}{\partial y} = \frac{\partial \psi}{\partial y} cos(\frac{\pi \hat{z}}{h_p}) \\ E_z &= -\frac{\partial \hat{\psi}}{\partial z} = -\frac{2}{h_p}\psi_0 - \frac{\pi}{h_p}\frac{\partial \psi}{\partial x} cos(\frac{\pi \hat{z}}{h_p}) \end{aligned} \tag{6}$$

$$H_x = -\frac{\partial \hat{\varphi}}{\partial x} = \frac{\partial \varphi}{\partial x} cos(\frac{\pi \hat{z}}{h_p}) \tag{7a}$$

$$H_y = -\frac{\partial \overset{\wedge}{\varphi}}{\partial y} = \frac{\partial \varphi}{\partial y} cos(\frac{\pi \hat{z}}{h_p}) \tag{7b}$$

$$H_z = -\frac{\partial \overset{\wedge}{\varphi}}{\partial z} = -\frac{2}{h_p}\varphi_0 - \frac{\pi}{h_p}\frac{\partial \varphi}{\partial x} cos(\frac{\pi \hat{z}}{h_p}) \tag{7c}$$

where ψ and φ are the electric and magnetic potentials, respectively, and expressed as follows: (Arefi and Zenkour 2017a, c, Ebrahimi and Barati 2019)

$$\begin{aligned} &\overset{\wedge}{\psi}(x,y,z,t) = -\frac{2\hat{z}}{h_p}\psi_0 - \psi(x,y,t)\, cos(\frac{\pi \hat{z}}{h_p}) \\ &\overset{\wedge}{\varphi}(x,y,z,t) = -\frac{2\hat{z}}{h_p}\varphi_0 - \varphi(x,y,t)\, cos(\frac{\pi \hat{z}}{h_p}) \\ &\hat{z} = z - \frac{h_c + h_p}{2}, \hat{z} = z + \frac{h_c + h_p}{2} \end{aligned} \tag{8}$$

In this study, four types distributions of porosity for porous core layer are considered as follows (Chen *et al.* 2016, Gao *et al.* 2018b, Ghasemi and Meskini 2019)

$$\begin{aligned} &Uniform\ distributions: \\ &\begin{cases} E(z) = E_1 - (1 - e_0\chi) \\ G(z) = G_1 - (1 - e_0\chi) \\ \rho(z) = \rho_1 - \sqrt{(1 - e_0\chi)} \end{cases} \end{aligned} \tag{9a}$$

$$\begin{aligned} &Symmetric\ distributions: \\ &\begin{cases} E(z) = E_1 - (1 - e_0\, cos(\frac{\pi z}{h})) \\ G(z) = G_1 - (1 - e_0\, cos(\frac{\pi z}{h})) \\ \rho(z) = \rho_1 - (1 - e_0\, cos(\frac{\pi z}{h})) \end{cases} \end{aligned} \tag{9b}$$

$$\begin{aligned} &Non\ symmetric\ stiff\ distributions: \\ &\begin{cases} E(z) = E_1 - (1 - e_0\, cos(\frac{\pi z}{2h} + \frac{\pi}{4})) \\ G(z) = G_1 - (1 - e_0\, cos(\frac{\pi z}{2h} + \frac{\pi}{4})) \\ \rho(z) = \rho_1 - (1 - e_0\, cos(\frac{\pi z}{2h} + \frac{\pi}{4})) \end{cases} \end{aligned} \tag{9c}$$

$$\begin{aligned} &Non\ symmetric\ soft\ distributions: \\ &\begin{cases} E(z) = E_1 - (1 - e_0\, sin(\frac{\pi z}{2h} + \frac{\pi}{4})) \\ G(z) = G_1 - (1 - e_0\, sin(\frac{\pi z}{2h} + \frac{\pi}{4})) \\ \rho(z) = \rho_1 - (1 - e_0\, sin(\frac{\pi z}{2h} + \frac{\pi}{4})) \end{cases} \end{aligned} \tag{9d}$$

where e_0 is porosity coefficients and e_m is mass density coefficients, in which, e_0, e_m and χ coefficients are written as follows (Barati and Zenkour 2017, Emdadi *et al.* 2019)

$$\begin{aligned} &e_0 = 1 - \frac{E_2}{E_1} = 1 - \frac{G_2}{G_1} \\ &e_m = 1 - \frac{\rho_2}{\rho_1} \\ &\frac{E_2}{E_1} = \left(\frac{\rho_2}{\rho_1}\right)^2 \end{aligned} \tag{10}$$

$$\begin{aligned} &e_m = 1 - \sqrt{1 - e_0} \\ &\chi = \frac{1}{e_0} - \frac{1}{e_0}\left(\frac{2}{\pi}\sqrt{1 - e_0} - \frac{2}{\pi} + 1\right)^2 \end{aligned} \tag{10}$$

The Hamilton's principle is used to obtain the relations of micro sandwich plate that is defined as follows (Reddy 2002, Mao and Zhang 2018)

$$\int \delta(T - U + W)dt = 0 \tag{11}$$

where T, U and W are kinetic energy, strain energy and external work, respectively. The kinetic energy and external work are defined as follows (Liu *et al.* 2013)

$$\begin{aligned} &\delta T = \int_v \rho v \delta \vec{v} dv \\ &\delta W = \int N^p \left(\left(\frac{\partial w}{\partial x}\right)^2 + \left(\frac{\partial w}{\partial y}\right)^2\right) dA \\ &N^p = -2e_{31}\psi_0 - 2q_{31}\varphi_0 \end{aligned} \tag{12}$$

Also, strain energy based on modified couple stress theory is considered as (Ke *et al.* 2012, Thai and Vo 2013)

$$\delta U = \frac{1}{2}\int (\sigma_{ij}\delta\varepsilon_{ij} + m_{ij}\delta\chi_{ij} - D_i\delta E_i - B_i\delta H_i)dV \tag{13}$$

in which σ_{ij},ε_{ij},m_{ij},χ_{ij},D_i,E_i,B_i ,H_i are the components of the stress tensor, the strain tensor, the deviatoric part of the symmetric couple stress tensor, the symmetric curvature tensor, the electric displacement, the electric fields, magnetic displacement and the magnetic fields, respectively. Also m_{ij} and$\chi_{ij}$are defined as follows (Sek *et al.* 2015, Mohammadimehr *et al.* 2017, Farokhi and Ghayesh 2018)

$$\begin{aligned} &m_{ij} = 2\mu l^2 \chi_{ij} \\ &\chi_{ij} = \frac{1}{2}(\nabla\theta_i + \nabla\theta_i{}^T) \end{aligned} \tag{14}$$

where l is the material length scale parameter and μ is Lame constant and θ_i are the components of the rotation vector related to the displacement field, that are defined as (Ghyesh *et al.* 2017)

$$\begin{aligned} &\theta_i = \frac{1}{2}(curl u)_i \\ &\mu = \frac{E(z)}{2(1+\nu)} \end{aligned} \tag{15}$$

where Poisson's ratio is a constant.

Also, the component of θ_i and χ_{ij} are defined in Appendix A. By substituting Eqs. (12), (13), (14), (15) into Eq. (11), the equilibrium equations are obtained as follows

$$\begin{aligned} \delta u_0:\quad &\frac{\partial N_{xx}}{\partial x} + \frac{\partial N_{xy}}{\partial y} + \frac{1}{2}\left[\frac{\partial^2 Q_{xz}}{\partial x \partial y} + \frac{\partial^2 Q_{yz}}{\partial y^2}\right] \\ &= I_1\frac{\partial^2 u}{\partial t^2} + I_2\frac{\partial^2 \varphi_x}{\partial t^2} \end{aligned} \tag{16}$$

$$\delta v_0: \quad \frac{\partial N_{xy}}{\partial x}+\frac{\partial N_{yy}}{\partial y}-\frac{1}{2}\left[\frac{\partial^2 Q_{xz}}{\partial x^2}+\frac{\partial^2 Q_{yz}}{\partial x\partial y}\right] = I_1\frac{\partial^2 v}{\partial t^2}+I_2\frac{\partial^2 \varphi_y}{\partial t^2}$$

$$\delta w_b: \quad k_s\frac{\partial N_{xz}}{\partial x}+k_s\frac{\partial N_{yz}}{\partial y} -\frac{1}{2}\left[\frac{\partial^2 Q_{xx}}{\partial x\partial y}-\frac{\partial^2 Q_{yy}}{\partial x\partial y}+\frac{\partial^2 Q_{xy}}{\partial y^2}-\frac{\partial^2 Q_{xy}}{\partial x^2}\right] = I_1\frac{\partial^2 w}{\partial t^2}$$

$$\delta \varphi_x: \quad \frac{\partial M_{xx}}{\partial x}+\frac{\partial M_{xy}}{\partial y}-k_sN_{xz} -\frac{1}{2}\left[-\frac{\partial Q_{yy}}{\partial y}+\frac{\partial Q_{zz}}{\partial y}-\frac{\partial Q_{xy}}{\partial x}-\frac{\partial^2 O_{xz}}{\partial x\partial y}-\frac{\partial^2 O_{yz}}{\partial y^2}\right] = I_3\frac{\partial^2 \varphi_x}{\partial t^2}I_2\frac{\partial^2 u}{\partial t^2} \tag{16}$$

$$\delta \varphi_y: \quad \frac{\partial M_{xy}}{\partial x}+\frac{\partial M_{yy}}{\partial y}-k_sN_{yz} -\frac{1}{2}\left[\frac{\partial Q_{xx}}{\partial x}-\frac{\partial Q_{zz}}{\partial x}+\frac{\partial Q_{xy}}{\partial y}+\frac{\partial^2 O_{xz}}{\partial x^2}+\frac{\partial^2 O_{yz}}{\partial x\partial y}\right] = I_3\frac{\partial^2 \varphi_y}{\partial t^2}I_2\frac{\partial^2 v}{\partial t^2}$$

$$\delta\psi: \quad \frac{\partial P_x}{\partial x}+\frac{\partial P_y}{\partial y}+P_z=0$$

$$\delta\varphi: \quad \frac{\partial R_x}{\partial x}+\frac{\partial R_y}{\partial y}+R_z=0$$

where

$$\begin{aligned}
&\int \sigma_{ij}dz = N_{ij} \quad (i,j=x,y)\\
&\int \sigma_{ij}zdz = M_{ij} \quad (i,j=x,y)\\
&\int D_i cos\left(\frac{\pi\hat{z}}{h_p}\right)dz = P_i \quad (i=x,y)\\
&\int B_i cos\left(\frac{\pi\hat{z}}{h_p}\right)dz = R_i \quad (i=x,y)\\
&\int B_i \frac{\pi}{h_p} sin\left(\frac{\pi\hat{z}}{h_p}\right)dz = R_i \quad (i=z)\\
&\int m_{ij}dz = Q_{ij} \quad (i,j=x,y,z)\\
&\int m_{ij}zdz = O_{ij} \quad (i,j=x,y,z)\\
&I_1,I_2,I_3 = \int \rho(1,z,z^2)dz
\end{aligned} \tag{17}$$

By substituting Eq. (17) into Eq. (16), the governing equations of motion for micro sandwich plate are obtained as follows

$$\begin{aligned}
\delta u: \quad & A_{11}\frac{\partial^2 u}{\partial x^2}+B_{11}\frac{\partial^2 \varphi_x}{\partial x^2}+A_{12}\frac{\partial^2 v}{\partial x\partial y}\\
&+B_{12}\frac{\partial^2 \varphi_y}{\partial x\partial y}+E_{13}\frac{\partial\psi}{\partial x}+F_{13}\frac{\partial\varphi}{\partial x}\\
&+A_{66}\frac{\partial^2 u}{\partial y^2}+A_{66}\frac{\partial^2 v}{\partial x\partial y}+B_{66}\frac{\partial^2 \varphi_x}{\partial y^2}\\
&+B_{66}\frac{\partial^2 \varphi_y}{\partial x\partial y}+\frac{1}{4}S_1\left(\frac{\partial^4 v}{\partial x^3\partial y}-\frac{\partial^4 u}{\partial x^2\partial y^2}\right)\\
&+\frac{1}{4}S_2\left(\frac{\partial^4 \varphi_y}{\partial x^3\partial y}-\frac{\partial^4 \varphi_x}{\partial x^2\partial y^2}\right)\\
&+\frac{1}{4}S_1\left(\frac{\partial^4 v}{\partial x\partial y^3}-\frac{\partial^4 u}{\partial y^4}\right)\\
&+\frac{1}{4}S_2\left(\frac{\partial^4 \varphi_y}{\partial x\partial y^3}-\frac{\partial^4 \varphi_x}{\partial y^4}\right)\\
&= I_1\frac{\partial^2 u}{\partial t^2}+I_2\frac{\partial^2 \varphi_x}{\partial t^2}
\end{aligned} \tag{18a}$$

$$\begin{aligned}
\delta v: \quad & A_{66}\frac{\partial^2 u}{\partial x\partial y}+A_{66}\frac{\partial^2 v}{\partial x^2}+B_{66}\frac{\partial^2 \varphi_x}{\partial x\partial y}\\
&+B_{66}\frac{\partial^2 \varphi_y}{\partial x^2}+A_{12}\frac{\partial^2 u}{\partial x\partial y}+B_{12}\frac{\partial^2 \varphi_x}{\partial x\partial y}\\
&+A_{22}\frac{\partial^2 v}{\partial y^2}+B_{22}\frac{\partial^2 \varphi_y}{\partial y^2}+E_{23}\frac{\partial\psi}{\partial y}+F_{23}\frac{\partial\varphi}{\partial y}\\
&+\frac{1}{4}S_1\left(-\frac{\partial^4 v}{\partial x^4}+\frac{\partial^4 u}{\partial x^3\partial y}\right)\\
&+\frac{1}{4}S_2\left(-\frac{\partial^4 \varphi_y}{\partial x^4}+\frac{\partial^4 \varphi_x}{\partial x^3\partial y}\right)\\
&+\frac{1}{4}S_1\left(-\frac{\partial^4 v}{\partial x^2\partial y^2}+\frac{\partial^4 u}{\partial x\partial y^3}\right)\\
&+\frac{1}{4}S_2\left(-\frac{\partial^4 \varphi_y}{\partial x^2\partial y^2}-\frac{\partial^4 \varphi_x}{\partial x\partial y^3}\right)\\
&= I_1\frac{\partial^2 v}{\partial t^2}+I_2\frac{\partial^2 \varphi_y}{\partial t^2}
\end{aligned} \tag{18b}$$

$$\begin{aligned}
\delta w: \quad & k_sA_{55}\frac{\partial^2 w}{\partial x^2}+k_sA_{55}\frac{\partial \varphi_x}{\partial x}-k_sG_{51}\frac{\partial^2 \psi}{\partial x^2}\\
&-k_sH_{51}\frac{\partial^2 \varphi}{\partial x^2}+k_sA_{44}\frac{\partial^2 w}{\partial y^2}+k_sA_{44}\frac{\partial \varphi_y}{\partial y}\\
&-k_sG_{52}\frac{\partial^2 \psi}{\partial y^2}-k_sH_{52}\frac{\partial^2 \varphi}{\partial y^2}\\
&+\frac{1}{2}S_1\left(-\frac{\partial^4 w}{\partial x^2\partial y^2}+\frac{\partial^3 \varphi_y}{\partial x^2\partial y}\right)\\
&+\frac{1}{2}S_1\left(\frac{\partial^3 \varphi_x}{\partial x\partial y^2}-\frac{\partial^4 w}{\partial x^2\partial y^2}\right)\\
&+\frac{1}{4}S_1\left(-\frac{\partial^4 w}{\partial y^4}+\frac{\partial^4 w}{\partial x^2\partial y^2}+\frac{\partial^3 \varphi_y}{\partial y^3}-\frac{\partial^3 \varphi_x}{\partial x\partial y^2}\right)\\
&+\frac{1}{4}S_1\left(\frac{\partial^4 w}{\partial x^2\partial y^2}-\frac{\partial^4 w}{\partial x^4}-\frac{\partial^3 \varphi_y}{\partial x^2\partial y}+\frac{\partial^3 \varphi_x}{\partial x^3}\right)\\
&= I_1\frac{\partial^2 w}{\partial t^2}
\end{aligned} \tag{18c}$$

$$\begin{aligned}
\delta \varphi_x: \quad & -k_sA_{55}\frac{\partial w}{\partial x}-k_sA_{55}\varphi_x+k_sG_{51}\frac{\partial\psi}{\partial x}\\
&+k_sH_{51}\frac{\partial\varphi}{\partial x}+\frac{1}{2}S_1\left(\frac{\partial^2 \varphi_x}{\partial y^2}-\frac{\partial^3 w}{\partial x\partial y^2}\right)\\
&+\frac{1}{2}S_1\left(-\frac{\partial^2 \varphi_y}{\partial x\partial y}+\frac{\partial^2 \varphi_x}{\partial y^2}\right)\\
&+\frac{1}{4}S_1\left(\frac{\partial^3 w}{\partial x\partial y^2}-\frac{\partial^3 w}{\partial x^3}-\frac{\partial^2 \varphi_y}{\partial x\partial y}+\frac{\partial^2 \varphi_x}{\partial x^2}\right)\\
&+\frac{1}{4}S_2\left(\frac{\partial^4 v}{\partial x^3\partial y}-\frac{\partial^4 u}{\partial x^2\partial y^2}\right)
\end{aligned} \tag{18d}$$

$$
\begin{aligned}
&+\frac{1}{4}S_3\left(\frac{\partial^4\varphi_y}{\partial x^3\partial y}-\frac{\partial^4\varphi_x}{\partial x^2\partial y^2}\right)\\
&+\frac{1}{4}S_2\left(\frac{\partial^4 v}{\partial x\partial y^3}-\frac{\partial^4 u}{\partial y^4}\right)\\
&+\frac{1}{4}S_3\left(\frac{\partial^4\varphi_y}{\partial x\partial y^3}-\frac{\partial^4\varphi_x}{\partial y^4}\right)\\
&-=I_2\frac{\partial^2 u}{\partial t^2}+I_3\frac{\partial^2\varphi_x}{\partial t^2}
\end{aligned}
\tag{18d}
$$

$$
\begin{aligned}
\delta\varphi_y:\quad & B_{12}\frac{\partial^2 u}{\partial x\partial y}+D_{12}\frac{\partial^2\varphi_x}{\partial x\partial y}+B_{22}\frac{\partial^2 v}{\partial y^2}\\
&+D_{22}\frac{\partial^2\varphi_y}{\partial y^2}+J_{23}\frac{\partial\psi}{\partial y}+K_{23}\frac{\partial\varphi}{\partial y}+B_{66}\frac{\partial^2 u}{\partial x\partial y}\\
&+B_{66}\frac{\partial^2 v}{\partial x^2}+D_{66}\frac{\partial^2\varphi_x}{\partial x\partial y}+D_{66}\frac{\partial^2\varphi_y}{\partial x^2}\\
&-k_sA_{44}\frac{\partial w}{\partial y}-k_sA_{44}\varphi_y+k_sG_{62}\frac{\partial\psi}{\partial y}\\
&+k_sH_{62}\frac{\partial\varphi}{\partial y}+\frac{1}{2}S_1\left(-\frac{\partial^3 w}{\partial x^2\partial y}+\frac{\partial^2\varphi_y}{\partial x^2}\right)\\
&+\frac{1}{2}S_1\left(\frac{\partial^2\varphi_y}{\partial x^2}-\frac{\partial^2\varphi_x}{\partial x\partial y}\right)\\
&+\frac{1}{4}S_1\left(-\frac{\partial^3 w}{\partial y^3}+\frac{\partial^3 w}{\partial x^2\partial y}+\frac{\partial^2\varphi_y}{\partial y^2}-\frac{\partial^2\varphi_x}{\partial x\partial y}\right)\\
&+\frac{1}{4}S_2\left(-\frac{\partial^4 v}{\partial x^4}+\frac{\partial^4 u}{\partial x^3\partial y}\right)\\
&+\frac{1}{4}S_3\left(-\frac{\partial^4\varphi_y}{\partial x^4}+\frac{\partial^4\varphi_x}{\partial x^3\partial y}\right)\\
&+\frac{1}{4}S_2\left(-\frac{\partial^4 v}{\partial x^2\partial y^2}+\frac{\partial^4 u}{\partial x\partial y^3}\right)\\
&+\frac{1}{4}S_3\left(-\frac{\partial^4\varphi_y}{\partial x^2\partial y^2}+\frac{\partial^4\varphi_x}{\partial x\partial y^3}\right)\\
&=I_2\frac{\partial^2 u}{\partial t^2}+I_3\frac{\partial^2\varphi_y}{\partial t^2}
\end{aligned}
\tag{18e}
$$

$$
\begin{aligned}
\delta\varphi:\quad & G_{51}\frac{\partial^2 w}{\partial x^2}+G_{51}\frac{\partial\varphi}{\partial x}+L_{11}\frac{\partial^2\psi}{\partial x^2}+N_{11}\frac{\partial^2\varphi}{\partial x^2}\\
&+G_{62}\frac{\partial^2 w}{\partial y^2}+G_{62}\frac{\partial\varphi_y}{\partial y}+L_{22}\frac{\partial^2\psi}{\partial y^2}\\
&+N_{22}\frac{\partial^2\varphi}{\partial y^2}+E_{31}\frac{\partial u}{\partial x}+J_{31}\frac{\partial\varphi_x}{\partial x}+E_{32}\frac{\partial v}{\partial y}\\
&+J_{32}\frac{\partial\varphi_y}{\partial y}-L_{33}^1-L_{33}\psi-N_{33}^1-N_{33}\varphi=0
\end{aligned}
\tag{18f}
$$

$$
\begin{aligned}
\delta\psi:\quad & H_{51}\frac{\partial^2 w}{\partial x^2}+H_{51}\frac{\partial\varphi_x}{\partial x}+N_{11}\frac{\partial^2\psi}{\partial x^2}+O_{11}\frac{\partial^2\varphi}{\partial x^2}\\
&+H_{62}\frac{\partial^2 w}{\partial y^2}+H_{62}\frac{\partial\varphi_y}{\partial y}+N_{22}\frac{\partial^2\psi}{\partial y^2}\\
&+O_{22}\frac{\partial^2\varphi}{\partial y^2}+F_{31}\frac{\partial u}{\partial x}+K_{31}\frac{\partial\varphi_x}{\partial x}+F_{32}\frac{\partial v}{\partial y}\\
&+K_{32}\frac{\partial\varphi_y}{\partial y}-N_{33}^2-N_{33}\psi-O_{33}^1-O_{33}\varphi=0
\end{aligned}
\tag{18g}
$$

where

$$
\begin{aligned}
&\int c_{ij}(1,z,z^2)dz=A_{ij},B_{ij},D_{ij}\\
&\int(e_{ij},q_{ij})\frac{\pi}{h_p}sin\left(\frac{\pi\hat{z}}{h_p}\right)dz=E_{ij},F_{ij}\\
&\int(e_{ij},q_{ij})cos\left(\frac{\pi\hat{z}}{h_p}\right)dz=G_{ij},H_{ij}\\
&\int(e_{ij},q_{ij})\frac{\pi}{h_p}sin\left(\frac{\pi\hat{z}}{h_p}\right)zdz=J_{ij},K_{ij}\\
&\int(\epsilon_{ii}\ m_{ii},\mu_{ii})\left(cos\left(\frac{\pi\hat{z}}{h_p}\right)\right)^2dz=L_{ii},N_{ii},O_{ii},\\
&\qquad\qquad\qquad\qquad (i=1),\\
&\int\mu_{ii}\left(\frac{\pi}{h_p}sin\left(\frac{\pi\hat{z}}{h_p}\right)\right)^2dz=O_{ii},\quad (i=3)
\end{aligned}
\tag{19}
$$

In this study, the Navier's method is used to solve the equations of motion for simply support boundary conditions, that these boundary conditions are expressed as (Farajpour *et al*. 2016, Arefi and Zenkour 2017a)

$$
\begin{aligned}
v_0=w_0=\varphi_x=\varphi_y=N_x=M_x=0\quad at\quad x=0,a\\
u_0=w_0=\varphi_x=\varphi_y=N_y=M_y=0\quad at\quad y=0,b
\end{aligned}
\tag{20}
$$

Also, based on Navier's method for simply support boundary condition, the displacements are defined (Farajpour *et al*. 2016, Arefi and Zenkour 2017a)

$$
\begin{aligned}
u(x,y,t)&=\sum_{m=1}^{\infty}\sum_{n=1}^{\infty}U_{mn}\,cos(\alpha x)\,sin(\lambda y)e^{i\omega t}\\
v(x,y,t)&=\sum_{m=1}^{\infty}\sum_{n=1}^{\infty}V_{mn}\,sin(\alpha x)\,cos(\lambda y)e^{i\omega t}\\
w(x,y,t)&=\sum_{m=1}^{\infty}\sum_{n=1}^{\infty}W_{mn}\,sin(\alpha x)\,sin(\lambda y)e^{i\omega t}\\
\varphi_x(x,y,t)&=\sum_{m=1}^{\infty}\sum_{n=1}^{\infty}\phi_{x_{mn}}\,cos(\alpha x)\,sin(\lambda y)e^{i\omega t}\\
\varphi_y(x,y,t)&=\sum_{m=1}^{\infty}\sum_{n=1}^{\infty}\phi_{y_{mn}}\,sin(\alpha x)\,cos(\lambda y)e^{i\omega t}\\
\psi(x,y,t)&=\sum_{m=1}^{\infty}\sum_{n=1}^{\infty}\psi_{mn}\,sin(\alpha x)\,sin(\lambda y)e^{i\omega t}\\
\varphi(x,y,t)&=\sum_{m=1}^{\infty}\sum_{n=1}^{\infty}\phi_{mn}\,sin(\alpha x)\,sin(\lambda y)e^{i\omega t}\\
\alpha&=\frac{m\pi}{a},\quad \lambda=\frac{n\pi}{b}
\end{aligned}
\tag{21}
$$

where m, n, ω are the axial and transverse wave numbers and natural frequency of vibration, respectively. Also, U, V, W, ϕ_x, ϕ_y, φ, ψ are unknown amplitudes. By substituting Eq. (21) into Eq. (18), the matrix form of equations for free vibration of micro sandwich plate is derived as follows

$$
\left([K]_{7\times7}-\omega^2[M]_{7\times7}\right)X_{7\times1}=0
\tag{22}
$$

Table 1 Properties of piezo electromagnetic ($BiTiO_3$-$CoFe_2O_4$) material

$c_{11}(GPa)$	$c_{22}(GPa)$	$c_{33}(GPa)$	$c_{12}(GPa)$	$c_{13}(GPa)$	$c_{23}(GPa)$	$c_{44}(GPa)$
226	226	216	125	125	124	44.2
$c_{55}(GPa)$	$c_{66}(GPa)$	$e_{31}(C/m^2)$	$e_{32}(C/m^2)$	$e_{51}(C/m^2)$	$e_{62}(C/m^2)$	$\in_{11}\ (C/Vm)$
44.2	50.5	-2.2	-2.2	5.8	5.8	6.5×10^{-9}
$\in_{22}\ (C/Vm)$	$\in_{33}\ (C/Vm)$	q_{13}	q_{23}	q_{51}	q_{62}	m_{11}
$\mathbf{6.5\times10^{-9}}$	6.5×10^{-9}	290.1	290.1	275	275	5.367×10^{-12}
m_{22}	m_{33}	μ_{11}	μ_{22}	μ_{33}	$\rho(kg/m^3)$	
$\mathbf{5.367\times10^{-12}}$	5.367×10^{-12}	-297×10^{-6}	-297×10^{-6}	83.5×10^{-6}	5550	

Table 2 Property of balsa wood

$E_{xx}(MPa)$	$E_{yy}(MPa)$	$E_{zz}(MPa)$	$G_{xy}(MPa)$	$G_{yz}(MPa)$
688.03	32.60	32.60	72.78	12.50
$G_{xz}(MPa)$	ν_{xy}	ν_{xz}	ν_{yz}	$\rho(kg/m^3)$
72.80	0.007	0.007	0.4797	90.987

The components of stiffness and mass matrices are presented in Appendix B. Also, for forced vibration analysis of micro sandwich plate, the external load can be illustrated as follows (Mohammadimehr and Rostami 2017)

$$p(x,y,t)=\sum_{m=1}^{\infty}\sum_{n=1}^{\infty}p_0\,sin(\Omega t)\,sin(\alpha x)\,sin(\lambda y) \tag{23}$$

where Ω is the frequency of forced vibration of micro plate. The deflection of micro sandwich plate for the micro sandwich plate is obtained as follows (Mohammadimehr and Rostami 2017)

$$\{U_{mn},V_{mn},W_{mn},\varphi_{x_{mn}},\varphi_{y_{mn}}\}^T = \frac{1}{\omega_n^2-\Omega^2}M^{-1}[0\quad 0\quad p_0\quad 0\quad 0]^T \tag{24}$$

The properties of piezo electro-magnetic material are presented in Table 1 that used in this research (Arefi and Zenkour 2017a).

Also, the property of balsa wood is presented in Table 2 (Newaz *et al*. 2016).

3. Numerical results and discussions

In this section, the result of the free vibration of micro sandwich plate with porous core layer and magneto-electric face sheets based on MCST and FSDT is presented. In the first, the obtained results by present study for FGM micro plate are compared with other research. The properties of FGM material for comparison between this research and the another articles are considered as $E=1.44\,GPa$, $\rho=1220\,(kg/m^3)$, $l=17.6\times10^{-6}$, $\nu=0.3$. Also, the non-dimensional natural frequency $\omega^*=\omega a^2/h\sqrt{\rho/E}$ is used to comparison the results of this study and other works. Table 3 indicates comparison of non-dimensional natural frequencies of micro plate in terms of various aspect ratio *a*/*h* and material length scale parameter to thickness ratio *l*/*h* based on the present and the obtained results by Ke *et al*. (2012) and Thai and Vo (2013). This comparison shows that the present numerical results are in good agreement with the obtained results by Ke *et al*. (2012) and Thai and Vo (2013). Also, the result is shown that with increasing of length to thickness ratio *a*/*h*, the non-dimensional natural frequencies increases and also, with an increase in the material length scale parameter to thickness ratio, the non-dimensional frequency enhances.

The effect of the thickness core layer to the total thickness of micro sandwich plate ratio (h_c/h) and side ratio (*a*/*b*) on the non-dimensional natural frequency of micro sandwich plate are presented in Fig. 2. The result indicates that with increasing of h_c/h, the non-dimensional frequency increases. Also, with an increase in the side ratio the non - dimensional frequency increases.

Fig. 3 shows the influence of h_c/h and aspect ratio (*b*/*h*) on the non-dimensional natural frequency of micro plate. The non- dimensional frequency increases with an increase in aspect ratio. Also, with increasing of the thickness of h_c/h, the non-dimensional frequency enhances. The results illustrated that with increasing of b/h and hc/h ratio, the stiffness of the plate becomes less and thus the natural frequency decreases; while the non-dimensional frequency is inversely proportional to aspect ratio, then it increases.

Table 3 Comparison of fundamental non dimensional frequency ω^* of micro plates with simply support boundary conditions

a/h	l/h	Present	Thai and Vo (2013)	Ke *et al.* (2012)
5	0.4	6.79	6.89	7.03
	0.8	9.63	10.02	10.67
	1	11.12	11.65	12.74
10	0.4	7.47	7.47	7.52
	0.8	10.77	11.01	11.23
	1	12.62	12.98	13.36
20	0.4	7.69	7.65	7.67
	0.8	11.16	11.34	11.41
	1	13.16	13.45	13.55

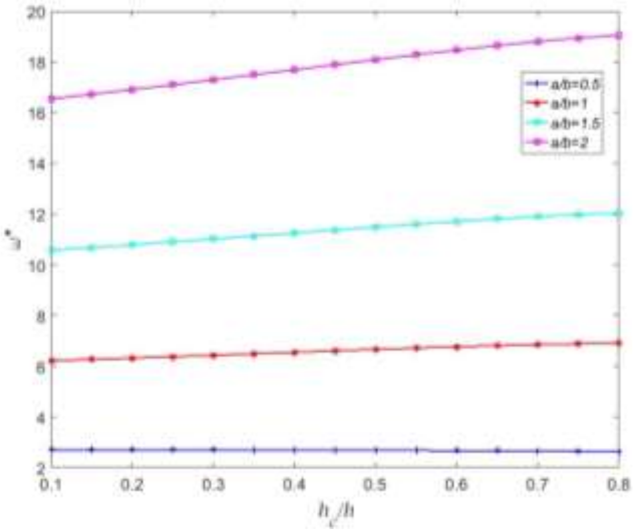

Fig. 2 Effect of h_c/h ratio and a/b ratio on the non-dimensional natural frequency of micro sandwich plate

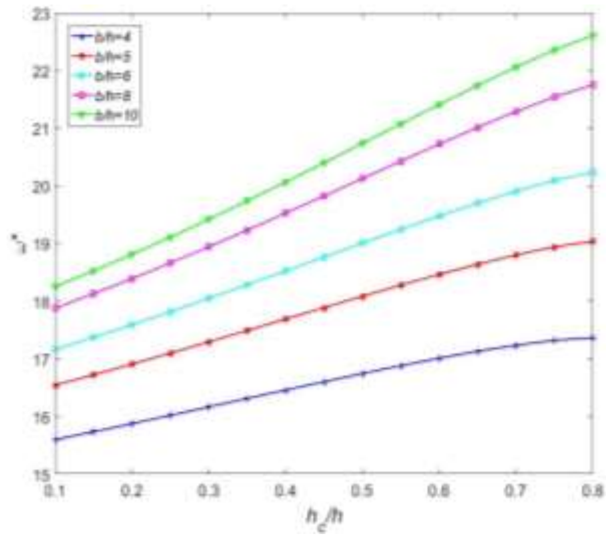

Fig. 4 Effect of h_c/h ratio and h/l ratio on the non-dimensional natural frequency of micro sandwich plate

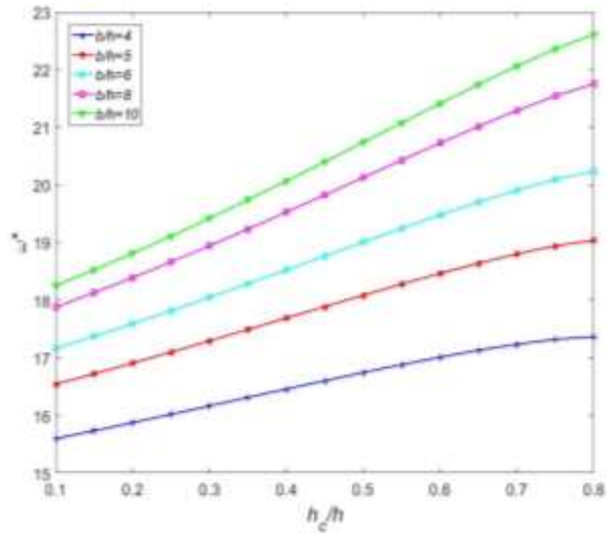

Fig. 3 Effect of h_c/h ratio and b/h ratio on the non-dimensional natural frequency of micro sandwich plate

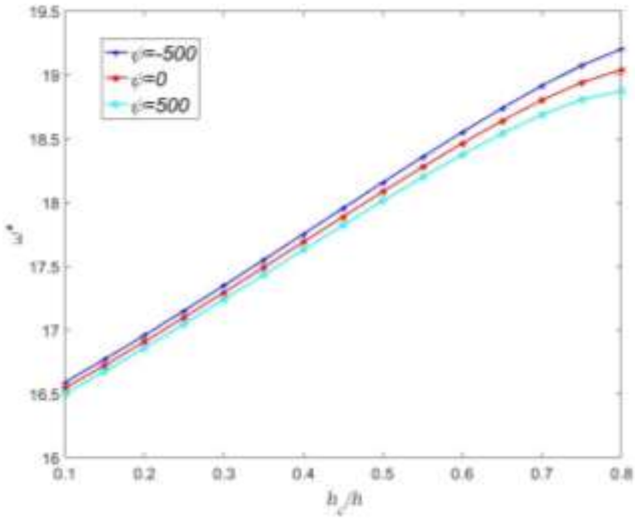

Fig. 5 Effect of h_c/h ratio and applied voltage on the non-dimensional natural frequency of micro sandwich plate

The influence of h_c/h and thickness of micro plate to material length scale parameter ratio (h/l) on the non-dimensional natural frequency of micro sandwich plate are expressed in Fig. 4. It can be concluded that with the increasing of h/l for micro sandwich plate, the non-dimensional frequency decreases. On the other hands, it is seen that with an increase in the thickness of micro plate to material length scale parameter ratio (h/l), the stiffness of the plate become more and while the non-dimensional frequency is inversely proportional to aspect ratio, then it decreases.

Fig. 5 illustrates the effect of applied voltage ψ on the non-dimensional natural frequency of micro sandwich plate. With increasing of the electric potential, the stiffness of micro structures decreases then it leads to decrease the natural frequency. The influence of applied magnetics potential φ on the non-dimensional natural frequency of micro sandwich plate is expressed in Fig. 6. It is observed that the non-dimensional frequency increases with increasing of the magnetic potential. Furthermore, with an increase in the thickness of piezo to thickness of the micro plate, the non-dimensional frequency increases. With increasing of the magnetic potential, the stiffness of micro structures increases then it leads to enhance the natural frequency. Fig. 7 presents the influence of porous coefficient on the non-dimensional natural frequency of micro sandwich plate. The numerical results are shown that with increasing of the porous coefficient, the non-dimensional frequency increases. Also, the non-dimensional frequency increases with increasing of the h_c/h ratio that

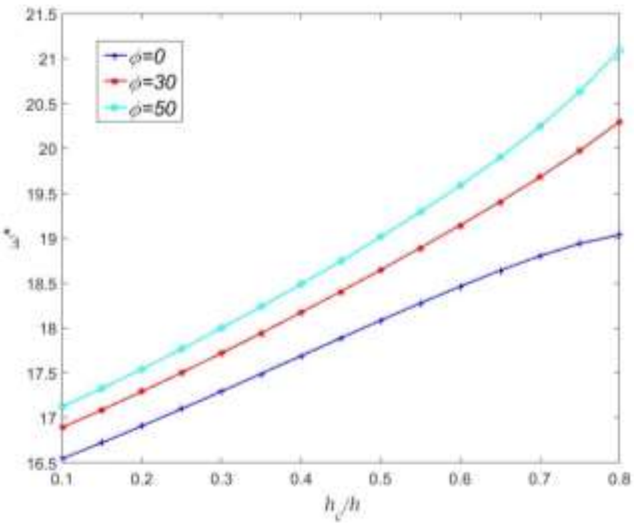

Fig. 6 Effect of h_c/h ratio and magnetic potentials on the non-dimensional natural frequency of micro sandwich plate

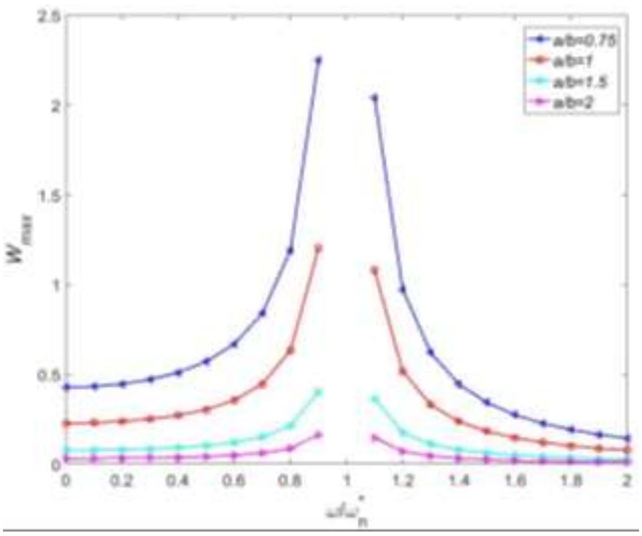

Fig. 8 Effect of length to width ratio (a/b) on the maximum deflection of micro sandwich plate

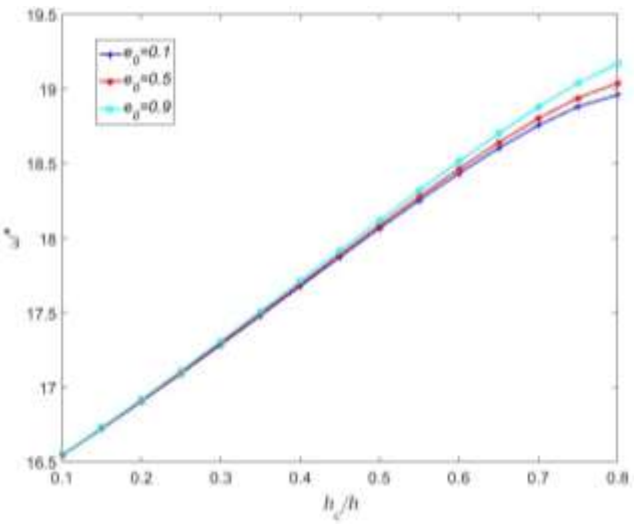

Fig. 7 Effect of h_c/h ratio and porous coefficient on the non-dimensional natural frequency of micro sandwich plate

difference between non dimensional frequencies with increasing of the h_c/h ratio increases.

Table 4 shows the influence of the type of porous with various h_c/h ratios on the non-dimensional frequency of micro sandwich plate. The result indicates that with increasing of the h_c/h ratio, the non-dimensional frequency increases. Also, for symmetric distributions of porous type, the non- dimensional frequency is larger than others distributions type of porous.

The influence of side ratio on the maximum deflection of micro sandwich plate is illustrated in Fig. 8. The maximum deflection decreases with increasing of side ratio. Also, with increasing of the frequency ratio, the maximum deflection in the first step increases and then decreases that maximum value of deflection occurs at frequency ratio equal to 1, which indicates a resonance phenomenon. Also with increasing of side ratio (a/b), micro sandwich plate will become a beam. It is known that the stiffness of plate is more than beam.

Fig. 9 presents the influence of the frequency ratio and width to thickness of piezo ratio on the maximum deflection of micro sandwich plate. The result indicates that maximum deflection with increasing of the aspect ratio decreases. Furthermore, with increasing of the frequency ratio, the maximum deflection increases and then decreases. That the peak of deflection occurs in the frequency ratio equal to 1. It is seen that with increasing of aspect ratio, the structure becomes softer.

The influence of thickness of micro sandwich plate to material length scale parameter ratio (h/l) and frequency ratio on the maximum deflection is considered in Figure 10. That with increasing of h/l, the maximum deflection of micro sandwich plate decreases. Also, with an increase in

Table 4 Effect type of porous on fundamental non dimensional frequency Ω of micro sandwich plates with various of h_c/h

Type of porous	**0.2**	**0.4**	**0.6**	**0.8**
Uniform	16.90736010	17.68935294	18.46355255	19.03821119
Symmetric	16.90740473	17.68952663	18.4640913	19.04000798
Non symmetric stiff	16.90739907	17.68947677	18.46388669	19.03924360
Non symmetric soft	16.90739450	17.68946421	18.46385781	19.03916761

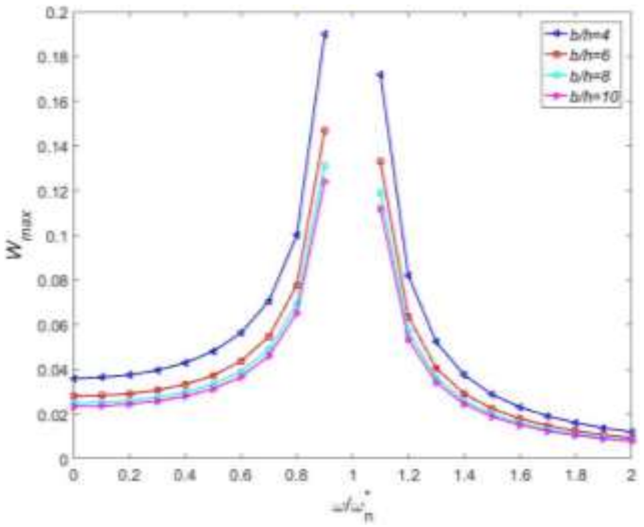

Fig. 9 Effect of width to thickness of piezo ratio (b/h) on the maximum deflection of micro sandwich plate

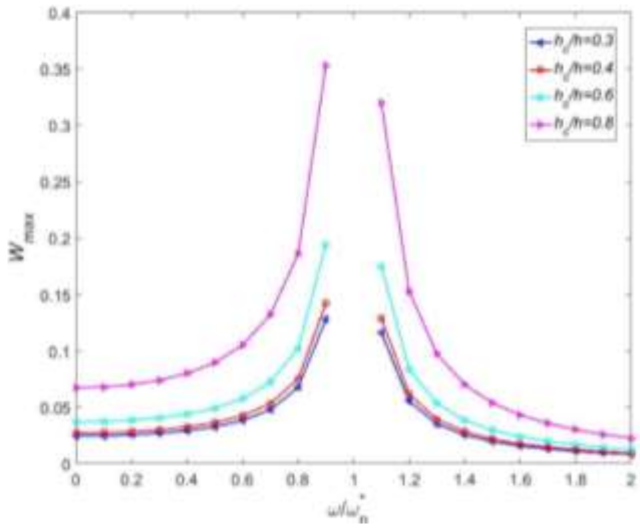

Fig. 11 Effect of h_c/h ratio on the maximum deflection of micro sandwich plate

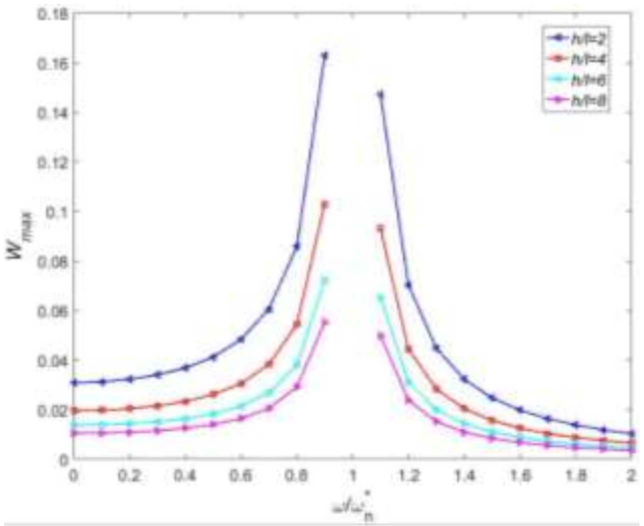

Fig. 10 Effect of width to thickness of piezo ratio (h/l) on the maximum deflection of micro sandwich plate

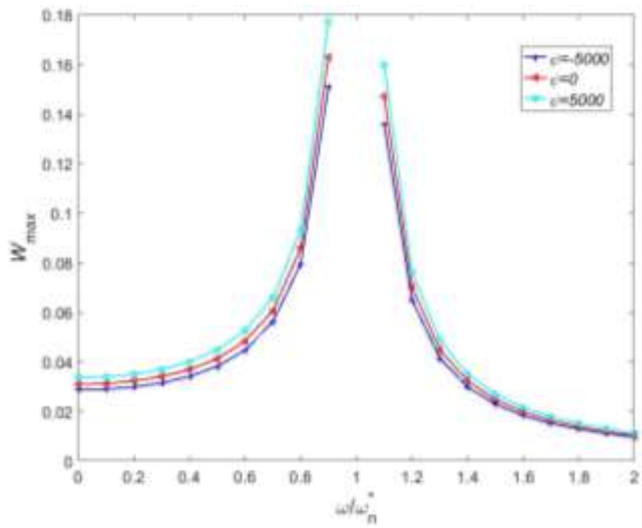

Fig. 12 Effect of electric potential and frequency ratio on the maximum deflection of micro sandwich plate

the frequency ratio, the maximum deflection in the first increases and then decreases that when the frequency ratio is equal to 1, the resonance phenomenon is occurred.

The effect of h_c/h and frequency ratio on the maximum deflection of micro sandwich plate is shown in Fig. 11. It is observed that with increasing of the thickness ratio, the maximum deflection increases. Also, the resonance is occurred at frequency ratio equal to 1. With increasing of the frequency ratio, the maximum deflection increases and then decreases. It can be seen from the figure that with increasing of h_c/h ratio, the stiffness of the plate becomes less. Moreover, increasing of thickness ratio leads to soft structures and thus the deflection of micro sandwich plate enhances.

Fig. 12 shows the influence of electric potential on the maximum deflection of micro sandwich plate. The result indicates that the maximum deflection of micro sandwich plate increases with increasing of the electric potential. With increasing of the electric potential, the stiffness of micro structures decreases then it leads to increase the deflection of sandwich plate. The influence of applied magnetics potential φ on the non-dimensional natural frequency of micro sandwich plate is expressed in Figure 6. It is observed that the non-dimensional frequency increases with increasing of the magnetic potential. Furthermore, with an increase in the thickness of piezo to thickness of the micro plate, the non-dimensional frequency increases. With increasing of the magnetic potential, the stiffness of micro structures increases then it leads to reduce the deflection of sandwich plate.

The effect of magnetic potential on the maximum deflection of micro sandwich plate is given in Fig. 13. With increasing of the magnetic potential, the maximum deflection decreases.

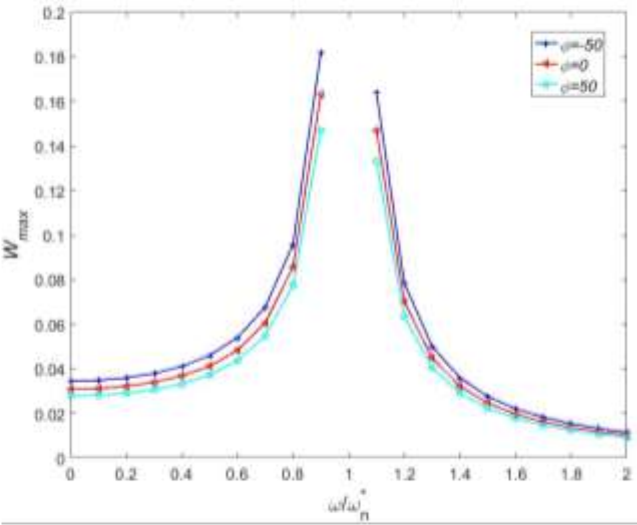

Fig. 13 Effect of magnetic potential and frequency ratio on the maximum deflection of micro sandwich plate

4. Conclusions

In this research, the influence of the electric potential and magnetic fields on the free and forced vibration of piezo magneto-electric micro sandwich plate with porous core layer is studied. Based on the FSDT and MCST, and using Hamilton's principle, the governing equations for micro sandwich plate are extracted. Then, for the simply support boundary condition, the Navier's solution is used to solve these equations. The result of this research are expressed as follows:

(1) The result indicates that with increasing of the thickness of core layer to total thickness of micro plate ratio, the non-dimensional frequency increases. Also with increasing of side ratio, the non -dimensional frequency increases. The results illustrated that with increasing of b/h and h_c/h ratio, the stiffness of the plate becomes less and thus the natural frequency decreases; while the non-dimensional frequency is inversely proportional to aspect ratio, then it increases.
(2) With an increase in the thickness of core layer to thickness of micro plate ratio, the non-dimensional frequency increases. It can be concluded that with the increasing of the thickness of micro plate to material length scale parameter ratio, the non-dimensional frequency decreases. The numerical results are shown that with increasing of the porous coefficient, the non-dimensional frequency increases.
(3) Based on the results the maximum deflection decreases with increasing of side ratio. Also, the maximum deflection with increasing of the aspect ratio decreases.
(4) With increasing of the thickness of core layer to total thickness of piezo ratio, the maximum deflection increases. Also, the resonance phenomenon has been occurred in the frequency ratio equal to 1.
(5) The result indicates that the maximum deflection of micro sandwich plate increases with increasing of the electric potential and vice versa for the magnetic potential. On the other hands, with an increase in the electric potential the micro structures becomes softer thus the deflection of sandwich plate increases and vice versa for magnetic potetials.

Acknowledgments

The authors would like to thank the referees for their valuable comments. Also, they are thankful to the Iranian Nanotechnology Development Committee for their financial support, and the University of Kashan for supporting this work by Grant No. 682561/20.

References

Abazid, M.A. and Sobhy, M. (2018), "Thermo-electro-mechanical bending of FG piezoelectric microplates on Pasternak foundation based on a four-variable plate model and the modified couple stress theory", *Microsyst. Technol.*, **24**(2), 1227-1245. https://doi.org/10.1007/s00542-017-3492-8

Arefi, M. and Zenkour, A.M. (2016), "Free vibration wave propagation and tension analyses of a sandwich micro nano rod subjected to electric potential using strain gradient theory", *Mater. Res. Exp.*, **3**(11), 115704. https://doi.org/10.1088/2053-1591/3/11/115704

Arefi, M. and Zenkour, A.M. (2017a), "Effect of thermos magneto- electromechanical fields on the bending behaviors of a three-layered nano plate based on sinusoidal shear deformation plate theory", *J. Sand. Struct. Mater.*, **21**(2), 639-669. https://doi.org/10.1177/1099636217697497

Arefi, M. and Zenkour, A.M. (2017b), "Electro-magneto-elastic analysis of a three-layer curved beam", *Smart. Struct. Syst., Int. J.*, **19**(6), 695-703. https://doi.org/10.12989/sss.2017.19.6.695

Arefi, M. and Zenkour, A.M. (2017c), "Nonlocal electro-thermo-mechanical analysis of a sandwich nanoplate containing a Kelvin–Voigt viscoelastic nanoplate and two piezoelectric layers", *Acta. Mech.*, **228**(2), 475-493. https://doi.org/10.1007/s00707-016-1716-0

Barati, M.R. and Zenkour, A.M. (2017), "Investigating post-buckling of geometrically imperfect metal foam nano beams with symmetric and asymmetric porosity distributions", *Compos. Struct.*, **182**, 91-98. https://doi.org/10.1016/j.compstruct.2017.09.008

Chen, D., Kitipornchai, S. and Yang, J. (2016), "Nonlinear free vibration of shear deformable sandwich beam with a functionally graded porous core", *Thin-wall. Struct.*, **107**, 39-48. https://doi.org/10.1016/j.tws.2016.05.025

Cong, P.H., Chien, T.M., Khoa, N.D. and Duc, N.D. (2018), "Nonlinear thermomechanical buckling and post-buckling response of porous FGM plates using Reddy's HSDT", *Aero. Sci. Tech.*, **77**, 419-428. https://doi.org/10.1016/j.ast.2018.03.020

Dong, Y.H., He, L.W., Wang, L., Li, Y.H. and Yang, J. (2018), "Buckling of spinning functionally graded graphene reinforced porous nanocomposite cylindrical shells: An analytical study", *Aero. Sci. Tech.*, **82-83**, 466-478. https://doi.org/10.1016/j.ast.2018.09.037

Ebrahimi, F. and Barati, M.R. (2019), "On static stability of electro-magnetically affected smart magneto-electro-elastic nanoplates", *Adv. Nano Res., Int. J.*, **7**(1), 63-75.

https://doi.org/10.12989/anr.2019.7.1.063

Emdadi, M., Mohammadimehr, M. and Navi, B.R. (2019), "Free vibration of an annular sandwich plate with CNTRC facesheets and FG porous cores using Ritz method", *Adv. Nano Res., Int. J.*, **7**(2), 109-123. https://doi.org/10.12989/anr.2019.7.2.109

Fakhari, V., Ohadi, A. and Yousefian, P. (2011), "Nonlinear free and forced vibration behavior of functionally graded plate with piezoelectric layer in thermal environment", *Compos. Struct.*, **93**, 2310-2321. https://doi.org/10.1016/j.compstruct.2011.03.019

Farajpour, A., Yazdi, M.R.H., Rastgoo, A., Loghmani, M. and Mohammadi, M. (2016), "Nonlocal nonlinear plate model for large amplitude vibration of magneto-electro-elastic nanoplates", *Compos. Struct.*, **140**, 323-336. https://doi.org/10.1016/j.compstruct.2015.12.039

Farokhi, H. and Ghayesh, M.H. (2018), "Modified couple stress theory in orthogonal curvilinear coordinates", *Acta. Mech.*, **230**(3), 851-869. https://doi.org/10.1007/s00707-018-2331-z

Gao, K., Gao, W., Chen, D. and Yang, J. (2018a), "Nonlinear free vibration of functionally graded graphene platelets reinforced porous nanocomposite plates resting on elastic foundation", *Comp. Struct.*, **204**, 831-846. https://doi.org/10.1016/j.compstruct.2018.08.013

Gao, K., Gao, W., Wu, B., Wu, D. and Song, C. (2018b), "Chongmin Song; Nonlinear primary resonance of functionally graded porous cylindrical shells using the method of multiple scales", *Thin-wall. Struct.* **125**, 281-293. https://doi.org/10.1016/j.tws.2017.12.039

Gao, K., Huang, Q., Kitipornchai, S. and Yang, J. (2019), "Nonlinear dynamic buckling of functionally graded porous beams", *Mech. Adv. Mater. Struct.*, 1-12. https://doi.org/10.1080/15376494.2019.1567888

Ghasemi, A.R. and Meskini, M. (2019), "Free vibration analysis of porous laminated rotating circular cylindrical shells", *J. Vib. Control*, **25**(18), 2494-2508. https://doi.org/10.1177/1077546319858227

Ghayesh, M.H., Farokhi, H., Hussain, S., Gholipour, A. and Arjomandi, M. (2017), "A size-dependent nonlinear third-order shear-deformable dynamic model for a microplate on an elastic medium", *Microsyst. Technol.*, **23**(8), 3281-3299. https://doi.org/10.1007/s00542-016-3096-8

Ghorbanpour Arani, A. and Zamani, M.H. (2018), "Nonlocal free vibration analysis of FG-porous shear and normal deformable sandwich nanoplate with piezoelectric face sheets resting on silica aerogel foundation", *Arab. J. Sci. Eng.*, **43**(9), 4675-4688. https://doi.org/10.1007/s13369-017-3035-8

Ghorbanpour Arani, A., Rousta Navi, B., Mohammadimehr, M. (2016), "Surface stress and agglomeration effects on nonlocal biaxial buckling polymeric nanocomposite plate reinforced by CNT using various approaches", *Adv. Compos. Mater.*, **25**(5), 423-441. https://doi.org/10.1080/09243046.2015.1052189

Ke, L.L., Wang, Y.S., Yang, J. and Kitipornchai, S. (2012), "Free vibration of size-dependent Mindlin microplates based on the modified couple stress theory", *J. Sound. Vib.*, **331**, 94-106. https://doi.org/10.1016/j.jsv.2011.08.020

Kim, J., Zur, K.K. and Reddy, J.N. (2019), "Bending, free vibration, and buckling of modified couples stress-based functionally graded porous micro-plates", *Compos. Struct.*, **209**, 879-888. https://doi.org/10.1016/j.compstruct.2018.11.023

Li, Y.S. and Pan, E. (2015), "Static bending and free vibration of a functionally graded piezo electric micro plate based on the modified couple-stress theory", *Int. J. Eng. Sci.*, **97**, 40-59. https://doi.org/10.1016/j.ijengsci.2015.08.009

Liu, C., Ke, L.L., Wang, Y.S., Yang, J. and Kitipornchai, S. (2013), "Thermo-electro-mechanical vibration of piezoelectric nanoplates based on the nonlocal theory", *Compos. Struct.*, **106**, 167-174. https://doi.org/10.1016/j.compstruct.2013.05.031

Mao, J.J. and Zhang, W. (2018), "Linear and nonlinear free and forced vibrations of graphene reinforced piezoelectric composite plate under external voltage excitation", *Compos. Struct.*, **203**, 551-565. https://doi.org/10.1016/j.compstruct.2018.06.076

Mohammadimehr, M. and Alimirzaei, S. (2016), "Nonlinear static and vibration analysis of Euler-Bernoulli composite beam model reinforced by FG-SWCNT with initial geometrical imperfection using FEM", *Struct. Eng. Mech., Int. J.*, **59**(3), 431-454. https://doi.org/10.12989/sem.2016.59.3.431

Mohammadimehr, M. and Rostami, R. (2017), "Bending buckling and forced vibration analysis of nonlocal nano compsite microplate using TSDT considering MEE properties dependent to various volume fractions of $CoFe_2O_4$-$BaTiO_3$", *J. Theo. Appl. Mech.*, **55**(3), 853-868. https://doi.org/10.15632/jtam-pl.55.3.853

Mohammadimehr, M., Mohandes, M. and Moradi, M. (2014), "Size dependent effect on the buckling and vibration analysis of double-bonded nanocomposite piezoelectric plate reinforced by boron nitride nanotube based on modified couple stress theory", *J. Vib. Control*, **22**(7), 1790-1807. https://doi.org/10.1177/1077546314544513

Mohammadimehr, M., Rousta Navi, B. and Ghorbanpour Arani, A. (2015), "Surface stress effect on the nonlocal biaxial buckling and bending analysis of polymeric piezoelectric nanoplate reinforced by CNT using eshelby-mori-tanaka approach", *J. Solid Mech.*, **7**(2), 173-190.

Mohammadimehr, M., Mohammadimehr, M.A. and Dashti, P. (2016), "Size-dependent effect on biaxial and shear nonlinear buckling analysis of nonlocal isotropic and orthotropic micro-plate based on surface stress and modified couple stress theories using differential quadrature method", *Appl. Mathe. Mech.*, **37**(4), 529-554. https://doi.org/10.1007/s10483-016-2045-9

Mohammadimehr, M., BabaAkbar, H.Z., Parakandeh, A. and Ghorbanpour Arani, A. (2017a), "Vibration analysis of double-bonded sandwich microplates with nanocomposite facesheets reinforced by symmetric and un-symmetric distributions of nanotubes under multi physical fields", *Struct. Eng. Mech., Int. J.*, **64**(3), 361-379. https://doi.org/10.12989/sem.2017.64.3.361

Mohammadimehr, M., Shahedi, S. and Rousta Navi, B. (2017b), "Nonlinear vibration analysis of FG-CNTRC sandwich Timoshenko beam based on modified couple stress theory subjected to longitudinal magnetic field using generalized differential quadrature method", *Proceedings of the Institution of Mechanical Engineers, Part C: J. Mech. Eng. Sci.*, **231**(20), 3866-3885. https://doi.org/10.1177/0954406216653622

Mohammadimehr, M., Navi, B.R. and Arani, A.G. (2017c), "Dynamic stability of modified strain gradient theory sinusoidal viscoelastic piezoelectric polymeric functionally graded single-walled carbon nanotubes reinforced nanocomposite plate considering surface stress and agglomeration effects under hydro-thermo-electro-magneto-mechanical loadings", *Mech. Adv. Mater. Structu.*, **24**(16), 1325-1342. https://doi.org/10.1080/15376494.2016.1227507

Mohammadimehr, M., Okhravi, S.V., Akhavan Alavi, S.M., (2018), "Free vibration analysis of magneto-electro-elastic cylindrical composite panel reinforced by various distributions of CNTs with considering open and closed circuits boundary conditions based on FSDT", *J. Vib. Control*, **24**(8), 1551-1569. https://doi.org/10.1177/1077546316664022

Mohandes, M. and Ghasemi, A.R. (2016), "Modified couple stress theory and finite strain assumption for nonlinear free vibration and bending of micro nano laminated composite Euler–Bernoulli beam under thermal loading", *Part C. J. Mech. Eng. Sci.*, **231**(21), 4044-4056. https://doi.org/10.1177/0954406216656884

Mojahedin, A., Jabbari, M., Khorshidvand, A.R. and Eslami, M.R. (2016), "Buckling analysis of functionally graded circular plates made of saturated porous materials based on higher order shear deformation theory", *Thin-wall. Struct.*, **99**, 83-90. https://doi.org/10.1016/j.tws.2015.11.008

Newaz, G., Mayeed, M. and Rasul, A. (2016), "Characterization of balsa wood mechanical properties required for continuum damage mechanics analysis", *J. Mater. Design. Appl.*, **230**(1), 206-218. https://doi.org/10.1177/1464420714564711

Razavi, S. and Shooshtari, A. (2015), "Nonlinear free vibration of magneto-electro-elastic rectangular plates", *Compos. Struct.*, **119**, 377-384. https://doi.org/10.1016/j.compstruct.2014.08.034

Reddy, J.N. (2002), *Energy Principles and Variational Methods in Applied Mechanics*, John Wiley & Sons, New Jersey, USA.

Rezaei, A.S. and Saidi, A.R. (2015), "Exact solution for free vibration of thick rectangular plates made of porous materials", *Compos. Struct.*, **134**, 1051-1060. https://doi.org/10.1016/j.compstruct.2015.08.125

Sasmal, S., Ravivarman, N., Sindu, B.S. and Vignesh, K. (2017), "Electrical conductivity and piezo-resistive characteristics of CNT and CNF incorporated cementitious nanocomposites under static and dynamic loading", *Compos. Part A. Appl. Sci. Manufact.*, **100**, 227-243. https://doi.org/10.1016/j.compositesa.2017.05.018

Sek, M.S., Aydın, M., Yurtcu, H.H. and Reddy, J.N. (2015), "Size-dependent vibration of a microplate under the action of a moving load based on the modified couple stress theory", *Acta. Mech.*, **226**(11), 3807-3822. https://doi.org/10.1007/s00707-015-1437-9

Selim, B.A., Yin, B.B. and Liew, K.M. (2108), "Impact analysis of CNT-reinforced composite plates integrated with piezoelectric layers based on Reddy's higher-order shear deformation theory", *Compos. Part B. Eng.*, **136**, 10-19. https://doi.org/10.1016/j.compositesb.2017.09.074

Shojaeefard, M.H., Googarchin, H.S., Ghadiri, M. and Mahinzare, M. (2017), "Micro temperature-dependent FG porous plate: Free vibration and thermal buckling analysis using modified couple stress theory with CPT and FSDT", *Appl. Math. Model.*, **50**, 633-655. https://doi.org/10.1016/j.apm.2017.06.022

Thai, H.T. and Vo, T.P. (2013), "A size-dependent functionally graded sinusoidal plate model based on a modified couple stress theory", *Compos. Struct.*, **96**, 376-383. https://doi.org/10.1016/j.compstruct.2012.09.025

Wang, Y., Feng, C., Santiuste, C., Zhao, Z. and Yang, J. (2019), "Buckling and postbuckling of dielectric composite beam reinforced with Graphene Platelets (GPLs)", *Aero. Sci. Tech*, **91**, 208-218. https://doi.org/10.1016/j.ast.2019.05.008

Yang, J., Chen, D. and Kitipornchai, S. (2018), "Buckling and free vibration analyses of functionally graded graphene reinforced porous nanocomposite plates based on Chebyshev-Ritz method", *Compos. Struct.*, **193**, 281-294. https://doi.org/10.1016/j.compstruct.2018.03.090

Zhang, Y.F., Zhang, W. and Yao, Z.G. (2018), "Analysis on nonlinear vibrations near internal resonances of a composite laminated piezoelectric rectangular plate", *Eng. Struct.*, **173**, 89-106. https://doi.org/10.1016/j.engstruct.2018.04.100

Zhao, J., Choe, K., Xie, F., Wang, A., Shuai, C. and Wang, Q. (2018), "Three-dimensional exact solution for vibration analysis of thick functionally graded porous (FGP) rectangular plates with arbitrary boundary conditions", *Compos. Part B. Eng.*, **155**, 369-381. https://doi.org/10.1016/j.compositesb.2018.09.001

CC

Nomenclature

a : length of plate
b : width of plate
h_c : thickness of core layer
h_p : thickness of piezo layers
c_{ij} : stiffness coefficients
e_{ij} : piezoelectric coefficients
q_{ij} : piezo magnetic coefficients
μ_{ij} : magnetic coefficients
$\in_{ii}$: dielectric coefficients
m_{ii} : electromagnetic coefficients
E_i : electric fields
H_i : magnetic fields
ψ : electric potentials
φ : magnetic potentials
E : modulus of elasticity
G : shear modulus
e_0 : porosity coefficients
e_m : mass density coefficients
T : kinetic energy
U : strain energy
W : external work
σ_{ij} : stress tensor
ε_{ij} : strain tensor
m_{ij} : symmetric couple stress tensor
χ_{ij} : symmetric curvature tensor
D_i : electric displacement
B_i : magnetic displacement
l : material length scale parameter
μ : Lame constant (shear modulus)
m : number of axial wave
n : number of transverse wave
ρ : Beam density
ω : natural frequency
K : stiffness matrix
M : mass matrix

Appendix A

$$\begin{aligned}\theta_x &= \frac{1}{2}\left(\frac{\partial w}{\partial y}-\varphi_y\right)\\ \theta_y &= \frac{1}{2}\left(\varphi_x-\frac{\partial w}{\partial x}\right)\\ \theta_x &= \frac{1}{2}\left[\left(\frac{\partial v}{\partial x}-\frac{\partial u}{\partial y}\right)+z\left(\frac{\partial \varphi_y}{\partial x}-\frac{\partial \varphi_x}{\partial y}\right)\right]\end{aligned} \tag{A1}$$

$$\begin{aligned}\chi_{yy} &= \frac{1}{2}\left(\frac{\partial \varphi_x}{\partial y}-\frac{\partial^2 w}{\partial x\partial y}\right)\\ \chi_{zz} &= \frac{1}{2}\left(\frac{\partial \varphi_y}{\partial x}-\frac{\partial \varphi_x}{\partial y}\right)\end{aligned} \tag{A2}$$

$$\begin{aligned}\chi_{xy} &= \frac{1}{4}\left[\frac{\partial^2 w}{\partial y^2}-\frac{\partial^2 w}{\partial x^2}-\frac{\partial \varphi_x}{\partial y}+\frac{\partial \varphi_x}{\partial x}\right]\\ \chi_{xz} &= \frac{1}{4}\left[\frac{\partial^2 v}{\partial x^2}-\frac{\partial^2 u}{\partial x\partial y}+z\left(\frac{\partial^2 \varphi_y}{\partial x^2}-\frac{\partial^2 \varphi_x}{\partial x\partial y}\right)\right]\\ \chi_{yz} &= \frac{1}{4}\left[\frac{\partial^2 v}{\partial x\partial y}-\frac{\partial^2 u}{\partial y^2}+z\left(\frac{\partial^2 \varphi_y}{\partial x\partial y}-\frac{\partial^2 \varphi_x}{\partial y^2}\right)\right]\end{aligned} \tag{A3}$$

Appendix B

$$\begin{aligned}X_{11} &= -\alpha^2 A_{11}-\lambda^2 A_{66}-\frac{1}{4}\alpha^2\lambda^2 S_1-\frac{1}{4}\lambda^4 S_1+I_1\omega^2\\ X_{12} &= -\alpha\lambda A_{12}-\alpha\lambda A_{66}+\frac{1}{4}\alpha^3\lambda S_1+\frac{1}{4}\alpha\lambda^3 S_1\\ X_{13} &= 0\\ X_{14} &= -\alpha^2 B_{11}-\lambda^2 B_{66}-\frac{1}{4}\alpha^2\lambda^2 S_2-\frac{1}{4}\lambda^4 S_2+I_2\omega^2\\ X_{15} &= -\alpha\lambda B_{12}-\alpha\lambda B_{66}+\frac{1}{4}\alpha^3\lambda S_2+\frac{1}{4}\alpha\lambda^3 S_2\\ X_{16} &= \alpha E_{13}\\ X_{17} &= \alpha F_{13}\end{aligned} \tag{B1}$$

$$\begin{aligned}X_{21} &= -\alpha\lambda A_{66}-\alpha\lambda A_{12}+\frac{1}{4}\alpha^3\lambda S_1+\frac{1}{4}\alpha\lambda^3 S_1\\ X_{22} &= -\alpha^2 A_{66}-\lambda^2 A_{22}-\frac{1}{4}\alpha^4 S_1-\frac{1}{4}\alpha^2\lambda^2 S_1+I_1\omega^2\\ X_{23} &= 0\\ X_{24} &= -\alpha\lambda B_{66}-\alpha\lambda B_{12}+\frac{1}{4}\alpha^3\lambda S_2+\frac{1}{4}\alpha\lambda^3 S_2\\ X_{25} &= -\alpha^2 B_{66}-\lambda^2 B_{22}-\frac{1}{4}\alpha^4 S_2-\frac{1}{4}\alpha^2\lambda^2 S_2+I_2\omega^2\\ X_{26} &= \lambda E_{23}\\ X_{27} &= \lambda F_{23}\end{aligned} \tag{B2}$$

$$\begin{aligned}X_{31} &= X_{32} = 0\\ X_{33} &= -k_s\alpha^2 A_{55}-k_s\lambda^2 A_{44}-\frac{1}{2}\alpha^2\lambda^2 S_1\\ &\quad -\frac{1}{2}\alpha^2\lambda^2 S_1-\frac{1}{4}\lambda^2 S_1+\frac{1}{4}\alpha^2\lambda^2 S_1\\ &\quad +\frac{1}{4}\alpha^2\lambda^2 S_1-\frac{1}{4}\alpha^4 S_1+I_1\omega^2\\ X_{34} &= -k_s\alpha A_{55}+\frac{1}{2}\alpha\lambda^2 S_1-\frac{1}{4}\alpha\lambda^2 S_1+\frac{1}{4}\alpha^3 S_1\\ X_{35} &= -k_s\alpha A_{44}+\frac{1}{2}\alpha^2\lambda S_1-\frac{1}{4}\alpha^2\lambda S_1+\frac{1}{4}\lambda^3 S_1\end{aligned} \tag{B3}$$

$$\begin{aligned}X_{36} &= k_s\alpha^2 G_{51}+k_s\lambda^2 G_{62}\\ X_{37} &= k_s\alpha^2 H_{51}+k_s\lambda^2 H_{62}\end{aligned} \tag{B3}$$

$$\begin{aligned}X_{41} &= -\alpha^2 B_{11}-\lambda^2 B_{66}-\frac{1}{4}\alpha^2\lambda^2 S_2-\frac{1}{4}\lambda^4 S_2+I_2\omega^2\\ X_{42} &= -\alpha\lambda B_{12}-\alpha\lambda B_{66}+\frac{1}{4}\alpha^3\lambda S_2+\frac{1}{4}\alpha\lambda^3 S_2\\ X_{43} &= -k_s\alpha A_{55}+\frac{1}{2}\alpha\lambda^2 S_1-\frac{1}{4}\alpha\lambda^2 S_1+\frac{1}{4}\alpha^3 S_1\\ X_{44} &= -\alpha^2 D_{11}-\lambda^2 D_{66}-k_s A_{55}\\ &\quad -\frac{1}{2}\lambda^2 S_1-\frac{1}{2}\lambda^2 S_1+I_3\omega^2-\frac{1}{4}\alpha^2 S_1\\ &\quad -\frac{1}{4}\alpha^2\lambda^2 S_3-\frac{1}{4}\lambda^4 S_3\\ X_{45} &= -\alpha\lambda D_{12}-\alpha\lambda D_{66}+\frac{1}{2}\alpha\lambda S_1\\ &\quad +\frac{1}{4}\alpha\lambda S_1+\frac{1}{4}\alpha^3\lambda S_3+\frac{1}{4}\alpha\lambda^3 S_3\\ X_{46} &= \alpha J_{13}+k_s\alpha G_{51}\\ X_{47} &= \alpha K_{13}+k_s\alpha H_{51}\end{aligned} \tag{B4}$$

$$\begin{aligned}X_{51} &= -\alpha\lambda B_{12}-\alpha\lambda B_{66}+\frac{1}{4}\alpha^3\lambda S_2+\frac{1}{4}\alpha\lambda^3 S_2\\ X_{52} &= -\lambda^2 B_{22}-\alpha^2 B_{66}-\frac{1}{4}\alpha^2\lambda^2 S_2-\frac{1}{4}\lambda^4 S_2+I_2\omega^2\\ X_{53} &= -k_s\lambda A_{44}+\frac{1}{2}\alpha^2\lambda S_1+\frac{1}{4}\lambda^3 S_1-\frac{1}{4}\alpha^2\lambda S_1\\ X_{54} &= -\alpha\lambda D_{12}-\alpha\lambda D_{66}+\frac{1}{2}\alpha\lambda S_1\\ &\quad +\frac{1}{4}\alpha\lambda S_1+\frac{1}{4}\alpha^3\lambda S_3+\frac{1}{4}\alpha\lambda^3 S_3\\ X_{55} &= -\lambda^2 D_{22}-\alpha^2 D_{66}-k_s A_{44}\\ &\quad -\frac{1}{2}\alpha^2 S_1-\frac{1}{2}\alpha^2 S_1-\frac{1}{4}\lambda^2 S_1\\ &\quad -\frac{1}{4}\alpha^4 S_3-\frac{1}{4}\alpha^2\lambda^2 S_3+I_3\omega^2\\ X_{56} &= \lambda J_{23}+k_s\lambda G_{62}\\ X_{57} &= \lambda K_{23}+k_s\lambda H_{62}\end{aligned} \tag{B5}$$

$$\begin{aligned}X_{61} &= -\alpha E_{31}\\ X_{62} &= -\lambda E_{32}\\ X_{63} &= -\alpha^2 G_{51}-\lambda^2 G_{62}\\ X_{64} &= -\alpha G_{51}-\alpha J_{31}\\ X_{65} &= -\lambda G_{62}-\lambda J_{32}\\ X_{66} &= -\alpha^2 L_{11}-\lambda^2 L_{22}-L_{33}\\ X_{67} &= -\alpha^2 N_{11}-\lambda^2 N_{22}-N_{33}\end{aligned} \tag{B6}$$

$$\begin{aligned}X_{71} &= -\alpha F_{31}\\ X_{72} &= -\lambda F_{32}\\ X_{73} &= -\alpha^2 H_{51}-\lambda^2 H_{62}\\ X_{74} &= -\alpha H_{51}-\alpha K_{31}\\ X_{75} &= -\lambda H_{62}-\lambda K_{32}\\ X_{76} &= -\alpha^2 N_{11}-\lambda^2 N_{22}-N_{33}\\ X_{77} &= -\alpha^2 O_{11}-\lambda^2 O_{22}-O_{33}\end{aligned} \tag{B7}$$